# Flight Dynamics of an Articulated Rotor Helicopter with an External Slung Load


Dario Fusato*
*Undergraduate Student*

Giorgio Guglieri
*Assistant Professor*

*Dipartimento di Ingegneria Aeronautica e Spaziale*
*Politecnico di Torino, Torino, Italy*

Roberto Celi
*Associate Professor*
*Alfred Gessow Rotorcraft Center*
*Department of Aerospace Engineering*
*University of Maryland, College Park, MD 20742*



**The paper presents a study of the flight dynamics of an articulated rotor helicopter carrying a suspended load. The aircraft model includes rigid body dynamics, individual flap and lag blade dynamics, and inflow dynamics. The load is a point mass with a single suspension point. Results were obtained for load masses of up to 2000 kg, with load-to-helicopter mass ratios of up to 28%, cable lengths from 3 to 8 m, turn rates of up to 16 deg/sec, and advance ratios of up to 0.3. The load affects trim primarily through the overall increase in the weight of the aircraft; the influence of cable length is negligible. Substantial coupling can occur between the Dutch roll and the load modes. Because of this coupling, the Dutch roll damping can decrease with a deterioration of handling qualities. The effects on the phugoid are very small. A suspended load modifies the roll frequency response by adding a notch to the gain curves and a 180-degree jump in the phase curves at the pendulum frequencies of the load. The changes in bandwidth and phase delay are small.**


## Notation

| | |
|---|---|
| $\mathbf{a}_L$ | absolute acceleration of the suspended load, Eq. (4) |
| $\mathbf{D}$ | aerodynamic force vector acting on the load, Eq. (6) |
| $\mathbf{F}_H$ | force applied by the load to the helicopter, Eq. (8) |
| $\mathbf{f}_L$ | vector of load equations of motion, Eq. (7) |
| $\mathbf{i}_B, \mathbf{j}_B, \mathbf{k}_B$ | unit vectors of the body axis coordinate system (Fig. 1) |
| $\mathbf{i}_G, \mathbf{j}_G, \mathbf{k}_G$ | unit vectors of the gravity axis system; the $\mathbf{k}_G$ vector is directed along the vertical |
| $\mathbf{i}_H, \mathbf{j}_H, \mathbf{k}_H$ | unit vectors of hook coordinate system (Fig. 1) |
| $l$ | cable length |
| $m$ | mass of the suspended load |
| $n_T$ | load factor |
| $p, q, r$ | roll, pitch, and yaw rate of the helicopter |
| $\mathbf{R}_H$ | position vector of the suspension point with respect to the aircraft CG, Eq. (2) |
| $\mathbf{R}_L$ | position vector of the load with respect to the suspension point, Eq. (1) |
| $S_L$ | equivalent flat plate area of the suspended load |
| $x_H, y_H, z_H$ | components of the position vector of the suspension point with respect to the aircraft center of mass (Fig. 1) |

*Greek Symbols and Subscripts*

| | |
|---|---|
| $\theta_F, \phi_F$ | pitch and roll angle of the fuselage |
| $\theta_L, \phi_L$ | coordinates of the suspended load (Fig. 1) |
| $\mu$ | advance ratio |
| $(\cdots)_0$ | trim value |


Manuscript received September 1998; accepted September 2000.


*Currently Graduate Research Assistant, Alfred Gessow Rotorcraft Center, University of Maryland, College Park, MD 20742.

## Introduction

Carrying external suspended loads has always been one of the traditional missions of the helicopter. Both military and commercial operators have exploited the capability of the helicopter to rapidly move heavy loads to locations where the use of ground based equipment would be impractical or impossible. The external load can modify the flight dynamic characteristics of a helicopter because the load behaves like a pendulum, and can change natural frequencies and mode shapes of the low frequency modes of the helicopter. Also, the aerodynamics of the load may make it unstable in certain flight conditions, with repercussions on the stability and the safety of the entire helicopter/load system.

The dynamics of a helicopter with external suspended loads received considerable attention in the late 1960's and early 1970's. Two reasons for this interest were the extensive external load operations in the Vietnam war, and the Heavy-Lift Helicopter program (HLH). This interest has been renewed recently, prompted by the re-evaluation and extension of the ADS-33 (Ref. 1) Helicopter Handling Qualities Specifications to transport helicopters, and in the expectation of new cargo helicopter procurements.

The first theoretical study of the dynamics of a helicopter with a slung load is probably due to Lucassen and Sterk (Ref. 2). A simple 3-degree of freedom model of the hover longitudinal dynamics of the helicopter and the angular displacement of the load was used. A single suspension point was assumed and the aerodynamic forces and moments on the load were neglected. In general, the pole of the load pendulum mode was stable; the phugoid remained unstable, but its frequency decreased with increasing cable length. For some combination of parameters the helicopter mode became unstable while the load mode was stabilized. Szustak and Jenney (Ref. 3) pointed out that a conventional stability augmentation system was not adequate for precision hover and load release, and could result

in pilot-induced oscillations (PIO). A more effective solution consisted of an inner loop in which the relative motion of aircraft and load was fed back to cyclic, and an outer loop with the aircraft position fed back, again to cyclic. Dukes studied the basic stability characteristics of a helicopter with a slung load, possible feedback stabilization schemes (Ref. 4), and appropriate piloting strategies for various maneuvers (Ref. 5). A 3-degree of freedom longitudinal helicopter/load model was used. Positive pitch damping, whether provided by the rotor alone or also by a flight control system, did not necessarily increase the stability of the pendulum mode of the load. This mode, essentially undamped, could become unstable for certain load configurations. Pitch damping provided at best a modest increase in the damping of the mode. A feedback scheme in which the attachment point was actively moved longitudinally proved effective on paper, but its practical feasibility was not explored.

The previous studies were limited to hover or low speed flight, and therefore the aerodynamics of the load did not play a significant role. Slung loads are rarely aerodynamically shaped bodies. The typical loads are bluff bodies that may be subject to dynamic instabilities triggered by unsteady aerodynamics. Poli and Cromack (Ref. 6) studied the stability in forward flight of a helicopter carrying an 8 ft $\times$ 8 ft $\times$ 20 ft container and a 20 ft long, 5.4 ft diameter circular cylinder. Long cables, high speeds, and low weights increased the stability of the loads. A stability study in forward flight by Cliff and Bailey (Ref. 7) partially confirmed the results of Ref. 6 because decreasing the weight improved stability, but longer cables were found to be destabilizing. The differences may be due to the different aerodynamics of the load, which was a much more idealized representation in Ref. 7. Lowering drag increased stability. Lateral-directional and longitudinal stability were governed by the same parameters, but the conditions for lateral stability proved more stringent.

A decade later, Nagabhushan again addressed the low-speed stability of a single-point suspension load configuration (Ref. 8). The analysis model was much more sophisticated than in any of the studies previously mentioned, and included full nonlinear equations for rigid body aircraft motion and rotor flap dynamics. The equations were then linearized for stability analysis, and the effect of several configuration parameters was investigated. Cable length, fore/aft and vertical position of the suspension point, and load weight were all found to affect stability. Depending on the combination of parameters some modes could be stabilized and others destabilized, but overall all the instabilities were quite weak.

More recently, Cicolani et al. have reported the results of flight tests of a UH-60 helicopter (Ref. 9), including frequency responses obtained using system identification techniques. While the study focused primarily on system identification and simulation validation, several conclusions were presented on the effect of the loads on flight dynamics and handling qualities. Increasing load weight reduced lateral bandwidth; further increases could reduce the bandwidth to a value below that of the pendulum frequency. Longitudinal stability margins were not very sensitive to the load, but lateral stability margins were degraded. The effect on bandwidth and phase delay was highly variable depending on the load configuration.

The general objective of the present paper is to explore some fundamental aspects of the dynamics of an articulated rotor helicopter with an external load suspended from a single attachment point. Therefore, the brief literature review presented above concerned this particular configuration. However, several studies have addressed the behavior of configurations with multiple attachment points. Reference will only be made here to an assessment of the state of the art for multi-point suspension configurations, presented by Sheldon (Ref. 10), to an in-depth theoretical study of the dynamics of a 2-suspension point, 4-cable load configuration subsequently carried out by Prabhakar (Ref. 11), and to a paper by Cicolani et al. (Ref. 12) which proposes a formulation valid for arbitrary numbers of aircraft, loads, and suspension points.

The specific objectives of this paper are:

1) To present the formulation and solution of the mathematical model of an articulated rotor helicopter carrying an external load, and

2) To study the effects of cable length and load weight on trim, stability, frequency response, and handling qualities characteristics of the helicopter, both in hover and forward flight, and both in straight flight and coordinated steady turns.

In the present study the load is modeled as a point mass that behaves like a spherical pendulum suspended from a single point. The only aerodynamic load is a quasi-steady drag force in the direction of the local airflow; no aerodynamic forces act on the cable. The cable is assumed to be massless and inelastic, that is, it does not bend and is axially rigid.

While this model is adequate for basic studies of the flight dynamics of helicopters with suspended loads, it cannot describe some important practical problems. Because the cable is inelastic, the sling load "vertical bounce" phenomenon (Ref. 13) cannot be modeled. This is a resonance condition that occurs when the natural frequency of the load is close to one of the rotor frequencies, and which requires an elastic cable model. Furthermore, the present model cannot capture the aerodynamic instabilities due to the non-streamlined shape of many suspended loads. These instabilities, described for example by Gabel and Wilson (Ref. 13), Poli and Cromack (Ref. 6), Sheldon (Ref. 10), and Simpson and Flower (Ref. 14), often limit the maximum speed of the helicopter. Finally, because it only assumes a single suspension point, the present model cannot be used to study the effects of number, spacing, and placement of suspension points, and the topology of the suspension cables. These parameters have been found to be very important for the stability and control characteristics of the helicopter, especially when the load has two or three nonnegligible dimensions, and therefore cannot be modeled as a point load; see, for example, the studies by Sheldon (Ref. 10), Prabhakar (Ref. 11), and Simpson and Flower (Ref. 14).

## Mathematical Model

### Modeling of the external load

The external load is essentially modeled as a point mass that behaves like a spherical pendulum suspended from a single point. The only aerodynamic load is a quasi-steady drag force in the direction of the local airflow; no aerodynamic forces act on the cable. The cable is assumed to be inelastic and with no mass.

*Load equations of motion.* The geometry and the relevant coordinate systems are shown in Fig. 1. The unit vectors $\mathbf{i}_H, \mathbf{j}_H, \mathbf{k}_H$ of the "hook" coordinate system always remain parallel to those of the body axis system $\mathbf{i}_B, \mathbf{j}_B, \mathbf{k}_B$. The position of the load is described by the two angles $\theta_L$ and $\phi_L$, where $\phi_L$ is the azimuth angle of the load and $\theta_L$ is measured from the $z_H$ axis. Therefore, the position vector $\mathbf{R}_L$ of the load with respect to the suspension point is given by:

$$\mathbf{R}_L = -l \sin\theta_L \cos\phi_L \mathbf{i}_H + l \sin\theta_L \sin\phi_L \mathbf{j}_H + l \cos\theta_L \mathbf{k}_H \tag{1}$$

The position vector $\mathbf{R}_H$ of the hook with respect to the aircraft c.g. is given by:

$$\mathbf{R}_H = x_H \mathbf{i}_H + y_H \mathbf{j}_H + z_H \mathbf{k}_H \tag{2}$$

The absolute velocity $\mathbf{V}_L$ of the load is given by:

$$\mathbf{V}_L = \mathbf{V}_{CG} + \dot{\mathbf{R}} + \boldsymbol{\Omega} \times \mathbf{R} \tag{3}$$

where $\mathbf{V}_{CG}$ is the absolute velocity of the center of mass of the helicopter, $\mathbf{R} = \mathbf{R}_L + \mathbf{R}_H$ is the position vector of the load with respect to the center of

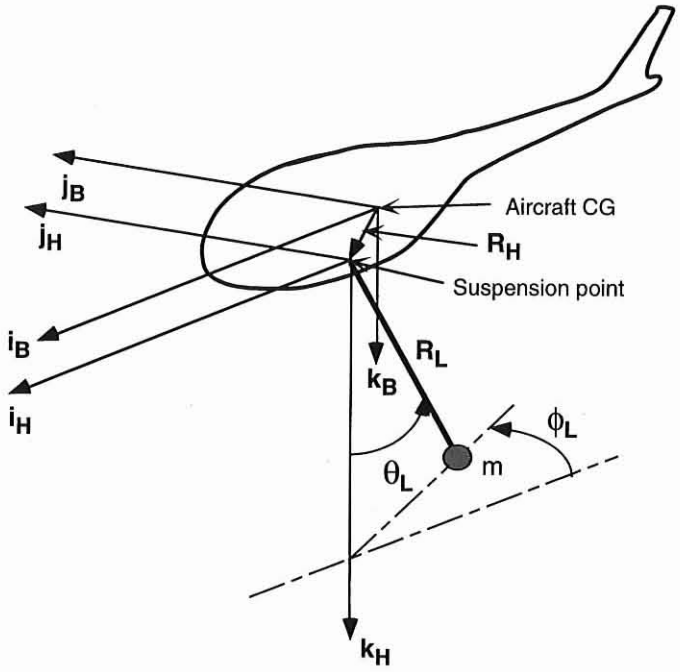


**Fig. 1. Geometry of suspended load.**

mass of the helicopter, and $\boldsymbol{\Omega} = p\mathbf{i}_B + q\mathbf{j}_B + r\mathbf{k}_B$ is the angular velocity. The absolute acceleration $\mathbf{a}_L$ of the load is:

$$\mathbf{a}_L = \mathbf{a}_{CG} + \ddot{\mathbf{R}} + \dot{\boldsymbol{\Omega}} \times \mathbf{R} + 2\boldsymbol{\Omega} \times \dot{\mathbf{R}} + \boldsymbol{\Omega} \times (\boldsymbol{\Omega} \times \mathbf{R}) \tag{4}$$

where $\mathbf{a}_{CG}$ is the absolute acceleration of the center of mass of the helicopter. The weight vector is given by:

$$mg\mathbf{k}_G = -mg \sin\theta_F \mathbf{i}_H + mg \sin\phi_F \cos\theta_F \mathbf{j}_H + mg \cos\phi_F \cos\theta_F \mathbf{k}_H \tag{5}$$

where $\mathbf{k}_G$ is the unit vector of the $z$-axis of a gravity reference frame, and $\phi_F$ and $\theta_F$ are respectively the roll and pitch attitudes of the fuselage. The aerodynamic force vector $\mathbf{D}$ contains only a drag contribution, and is given by:

$$\mathbf{D} = \frac{1}{2}\rho |\mathbf{V}_L| \mathbf{V}_L S_L \tag{6}$$

where $S_L$ is the equivalent flat plate area of the suspended load.

The equations of motion of the load are written by enforcing moment equilibrium about the suspension point, that is, in matrix form:

$$\mathbf{f}_L(\phi_L, \theta_L; \mathbf{q}_H) = -\mathbf{R}_L \times (-m\mathbf{a}_L + mg\mathbf{k}_G + \mathbf{D}) = 0 \tag{7}$$

where $\mathbf{q}_H$ is a vector of helicopter states. In scalar form, Eq. (7) is a system of three second order equations in the load coordinates $\phi_L$ and $\theta_L$. Only two (any two) of these equations need to be retained in the solution.

*Load contributions to rigid body equations of motion.* The suspended load introduces additional terms in the rigid body force and moment equations of motion of the helicopter. These terms are of inertial and aerodynamic origin.

The force $\mathbf{F}_H$ that the load exerts on the helicopter is given by:

$$\mathbf{F}_H = -m\mathbf{a}_L + \mathbf{D} + mg\mathbf{k}_G \tag{8}$$

The additional moment $\mathbf{M}_H$ is therefore given by:

$$\mathbf{M}_H = \mathbf{R}_H \times \mathbf{F}_H \tag{9}$$

Both $\mathbf{F}_H$ and $\mathbf{M}_H$ are functions of $\theta_L$ and $\phi_L$, and of all the fuselage and rotor states.

### Modeling of the helicopter

The mathematical model of the helicopter used in this study is a nonlinear blade element type model that includes fuselage, rotor, and main rotor inflow dynamics. The 6 degree of freedom rigid body motion of the aircraft is modeled using nonlinear Euler equations. Linear aerodynamics is assumed for fuselage and empennage. An articulated, four-bladed main rotor with rigid blades is assumed. Unsteady aerodynamic effects are modeled using the Pitt-Peters dynamic inflow model (Ref. 15).

The coupled system of rotor, fuselage, and inflow equations of motion is written in first-order form. The state vector has a total of 32 elements: flap and lag displacements and rates for each of the 4 blades (16 states); 9 rigid body velocities, rates, and attitudes; 3 inflow states; and 2 external load angles with their respective rates.

## Solution Technique

### Trim procedure

The trim procedure is the same as in Refs. 16, 17. Thus, the rotor equations of motion are transformed into a system of nonlinear algebraic equations using a Galerkin method. The algebraic equations enforcing force and moment equilibrium, and additional kinematic equations that must be satisfied in a turn, are added to the rotor equations, and the combined system is solved simultaneously. The solution yields the harmonics of a Fourier expansion of the rotor degrees of freedom, the pitch control settings, trim attitudes and rates of the entire helicopter, and main and tail rotor inflow. Two algebraic equations for the trim of the load are obtained from Eqs. (7) by setting the accelerations $\ddot{\phi}_L$ and $\ddot{\theta}_L$ to zero. The aircraft states that appear in the acceleration $\mathbf{a}_L$ of the load are also set to their trim values.

A spherical pendulum with a fixed attachment point, no dissipative applied forces, and $\theta_L$ measured from the downward vertical, has two types of equilibrium conditions (Ref. 18). The first corresponds to a zero trim value $\dot{\phi}_{L0}$ of $\dot{\phi}_L$, which implies that the pendulum oscillates in a plane. If it is also $\dot{\theta}_{L0} = 0$, then the pendulum is stationary. The second equilibrium condition corresponds to $\dot{\phi}_{L0} \neq 0$, that is, the pendulum rotates at constant speed around the vertical axis. The trim formulation of this study only yields the first type of equilibrium condition with $\dot{\phi}_{L0} = \dot{\theta}_{L0} = 0$, that is, the load is stationary with respect to the "hook" or the body axis system. The second equilibrium cannot be realized in practice because the dissipative effect of drag would not allow $\dot{\phi}_{L0}$ to be constant: the load trajectory would be a spiral of decreasing radius. Even if drag could be neglected, and a constant, nonzero $\dot{\phi}_{L0}$ could be assumed, the trim formulation of this study would still be unable to describe this equilibrium motion because it is based on the assumption that the linear and angular accelerations of the fuselage are zero. With a rotating external load this will not be possible because the applied forces and moments will be periodic. By appropriately moving the controls a pilot may still be able to keep the helicopter in a steady flight condition, at least in an average sense, with a moving load underneath. This, however, is not a rigorous trimmed condition and the trim formulation used in the present study is no longer valid.

### Linearization

Small perturbation equations are obtained by numerical linearization of the nonlinear equations about a trimmed condition. A multiblade coordinate transformation is used to transform the blade equations into a

nonrotating coordinate system. The transformation removes most of the periodicity of the equations; the residual periodic terms are averaged over one rotor revolution, so that the final linearized system is time invariant. This system is used to calculate frequency responses, poles and zeros. The suspended load adds two oscillatory modes. They can be visualized as coupled oscillations in two mutually perpendicular planes, or as an oscillation contained in a plane that is also rotating.

## Results

The helicopter configuration selected for this study is representative of a UH-60 Black Hawk. The weight without the external load is 7258 kg (16000 lbs), corresponding to a $C_T/\sigma = 0.07$. The altitude for all the results is 30.5 m (100 ft). The cable lengths considered are $l = 3$, 5, and 8 m, the load masses, $m = 500$, 1000, and 2000 kg, and the advance ratio, $\mu$, from 0 to 0.3, corresponding to airspeeds from 0 to 129 kts. For the purpose of calculating drag, the load is assumed to have an equivalent flat plate area $S_L = 0.4$ m$^2$. The 5-meter cable length and the values of the mass are comparable to those of the CONEX loads used in Ref. 9, although the aerodynamic shapes of the two types of load are very different.

### Trim results

Figures 2 and 3 show the position of the load with respect to the suspension point. The $x$ and $y$ distances are measured in the "hook" coordinate system, and therefore show how an observer on the helicopter would see the load looking down from the location of the hook. Therefore, a load aligned with the $z_H$ axis would have both coordinates equal to zero.

Figure 2 shows the effect of advance ratio for three combinations of cable length and load mass. In hover the cable is vertical. However, the $y$ coordinate of the load is negative because the helicopter is banked to the left. The position of the loads for the $l = 5$ case is almost the same in hover, because the bank angle is almost the same. The larger distance from the hook axis of the $l = 8$, $m = 1000$ case, compared with the $l = 5$, $m = 1000$ case is a geometric effect due to the longer cable. As $\mu$ increases, the load appears to move forward: this is primarily due to an increase in nose-down pitch of the helicopter. At higher speeds the growing effect of drag makes the load move back despite a further increase in nose-down pitch attitude. For $\mu \geq 0.1$ the helicopter is trimmed with zero roll angle $\phi_F$ and variable sideslip $\beta$. Because the value of $\beta$ is relatively small, the drag acts almost parallel to the $x$ body axis. This, together with $\phi_F = 0$, makes the load move close to the $x$-$y$ plane.

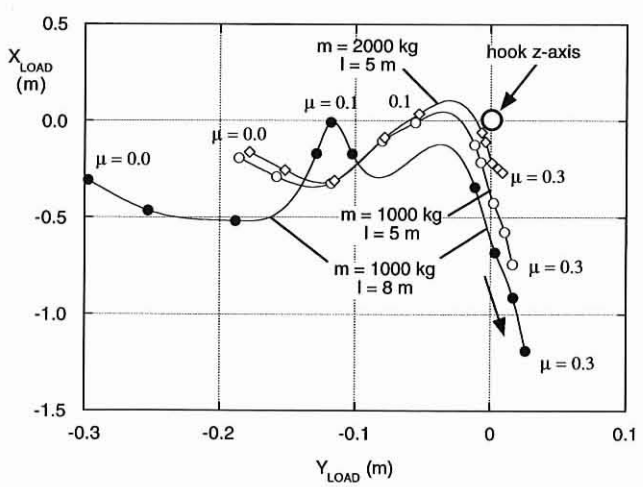


**Fig. 2. Displacement of suspended load in trimmed flight as a function of advance ratio $\mu$ for three different load configurations; $\Delta\mu = 0.025$ for $\mu \leq 0.15$, and $\Delta\mu = 0.05$ for $0.15 \leq \mu \leq 0.3$.**

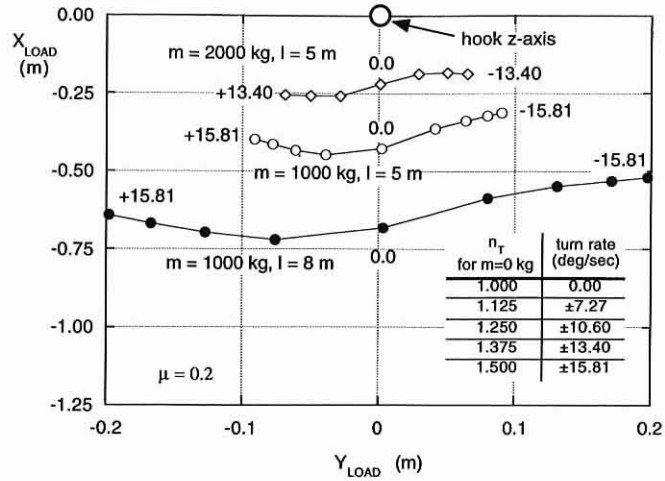


**Fig. 3. Displacement of suspended load in trimmed flight as a function of turn rate and load factor $n_T$ for three different load configurations.**

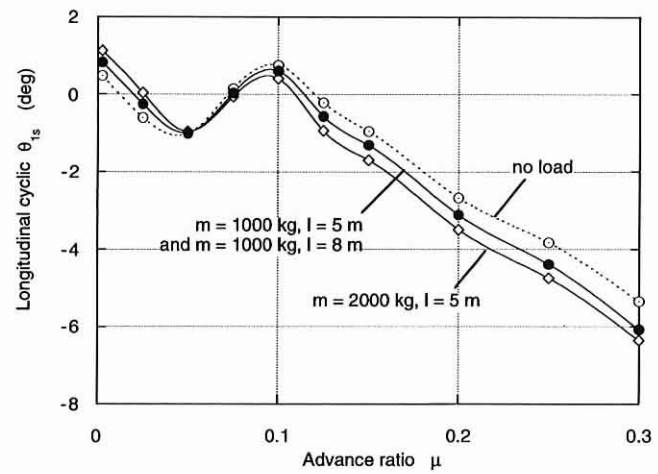


**Fig. 4. Trim value of longitudinal cyclic pitch as a function of advance ratio $\mu$ for three different load configurations.**

Figure 3 shows the $x$-$y$ load displacement in steady turns at an advance ratio $\mu = 0.2$ for increasing load factor. The points on the curves are for the turn rates indicated in the table added to the figure. Without the external load these values correspond to load factors $n_T$ increasing from 1 to 1.5 in increments of 0.125. For the configurations with external loads the values of $n_T$ should be increased in proportion to the increase in overall weight due to the load. It was not possible to trim the helicopter with the 2000 kg load at turn rates of $\pm 15.81$ deg/sec, which correspond to a load factor of about 1.9. The figure shows that the load remains very close to the $x$-$y$ plane even as the plane moves in space due to the increasing roll angle of the fuselage. Because of centrifugal force effects, the load moves slightly to the left of the plane in right-handed turns (positive turn rate), and to the right for left-handed turns. The longitudinal position of the load also remains largely unchanged.

Figures 4 and 5 show the trim values of longitudinal and lateral cyclic pitch respectively, as a function of the advance ratio $\mu$, and for three different load configurations. It should be pointed out that the trim algorithm sets the sideslip angle $\beta$ to zero and leaves the roll angle $\phi_F$ variable at low speed ($\mu < 0.1$). At higher speed, the turn coordination equation for zero

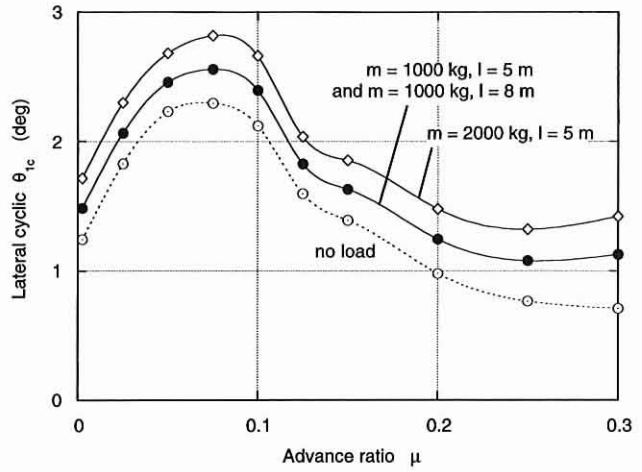


**Fig. 5. Trim value of lateral cyclic pitch as a function of advance ratio $\mu$ for three different load configurations.**

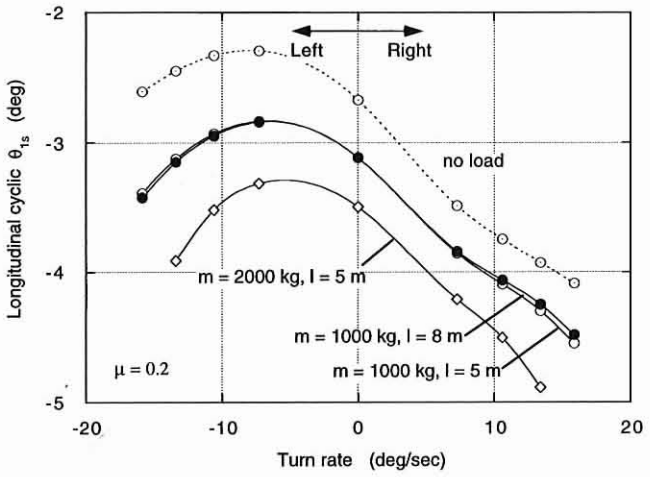


**Fig. 6. Trim value of longitudinal cyclic pitch as a function of turn rate for three different load configurations; advance ratio is $\mu = 0.2$.**

turn rate sets the value of $\phi_F$ so as to satisfy $\sin\phi_F \cos\theta_F = 0$. Figure 4 indicates that larger negative values of longitudinal cyclic are required as the load increases, for $\mu > 0.1$. This, however, is mostly due to the increase in overall weight due to the external load, and only in small part to the additional drag force generated by the load. At low speed a slightly more aft longitudinal cyclic is needed. Figure 5 shows that a higher value of lateral cyclic, corresponding to the stick more to the left, is required as the load increases. This increase is mostly due to the increase in overall weight of the helicopter, and persists at all values of $\mu$. Cable length does not have any influence, because it does not enter the force equilibrium and does not change the line of action of the forces exerted by the load on the helicopter.

Figures 6 and 7 show the trim values of longitudinal and lateral cyclic pitch respectively, as a function of turn rate, and for three different load configurations, at an advance ratio $\mu = 0.2$. More forward and left stick is required with increasing load mass for all turn rates and in either turn direction. The load affects the trim values primarily through the increase in the overall helicopter weight. This is indicated by the minimal effect of cable length, by changes in cyclic pitch essentially proportional to load weight, and by the fact that the load remains very close to the $x$-$y$ plane regardless of the value of $\phi_F$, as previously observed. Some effects

**Table 1. Effect of model complexity on frequency and damping of selected modes in hover; $m = 1000$ kg, $l = 5$ m**

| Model Type | Damping Ratio | Frequency (rad/sec) |
|---|---|---|
| Phugoid | | |
| RB | −0.32587 | 0.54075 |
| RB-R | −0.32304 | 0.53641 |
| RB-R-I | −0.32388 | 0.53124 |
| Dutch roll | | |
| RB | 0.26243 | 0.64462 |
| RB-R | 0.27528 | 0.64578 |
| RB-R-I | 0.26824 | 0.64849 |
| First load mode | | |
| RB | 0.16419 | 1.5299 |
| RB-R | 0.17294 | 1.4760 |
| RB-R-I | 0.17081 | 1.4615 |
| Second load mode | | |
| RB | 0.019550 | 1.5907 |
| RB-R | 0.020940 | 1.5942 |
| RB-R-I | 0.021210 | 1.5959 |

Key to model type:
RB → 6-DOF rigid body (13 states)
RB-R → 6-DOF rigid body plus rotor (29 states)
RB-R-I → 6-DOF rigid body plus rotor and inflow (32 states)
(All models include 4 slung load states)

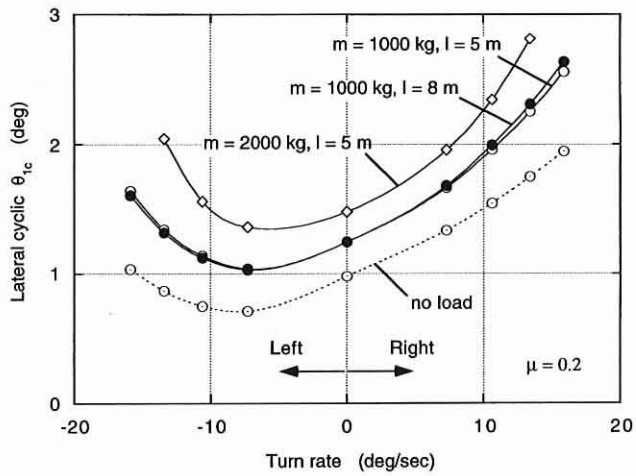


**Fig. 7. Trim value of lateral cyclic pitch as a function of turn rate for three different load configurations; advance ratio is $\mu = 0.2$.**

of cable length can be seen at the higher turn rates, but they are very small.

### Stability results

All the results presented in this section have been obtained with a model that includes rotor and inflow dynamics, for a total of 32 states. For the articulated rotor configuration used in this study, rotor and inflow dynamics have a modest influence on the frequency and damping of the rigid body and the suspended load modes. Table 1 shows typical results. The data are for a hover condition with a load mass $m = 1000$ kg and a cable length $l = 5$ m. Frequency and damping of the phugoid, Dutch roll, and first and second load modes (which are mostly a lateral and a longitudinal oscillation of the load respectively) do not change by more than about 5% when rotor and inflow dynamics are taken into account.

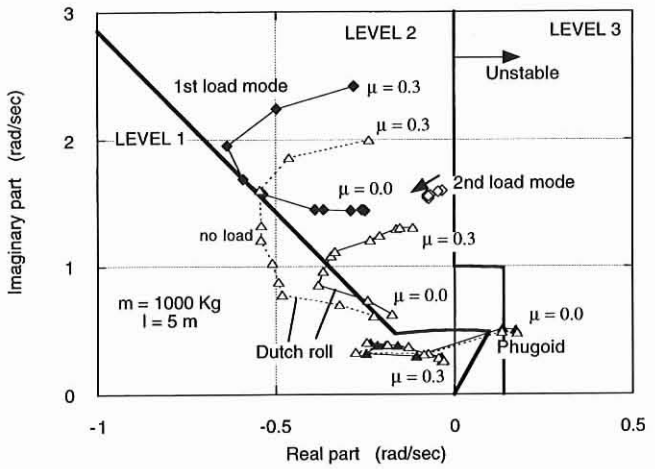


**Fig. 8. Selected aircraft and load poles as a function of advance ratio $\mu$; $\Delta\mu = 0.025$ for $\mu \leq 0.15$, and $\Delta\mu = 0.05$ for $0.15 \leq \mu \leq 0.3$.**

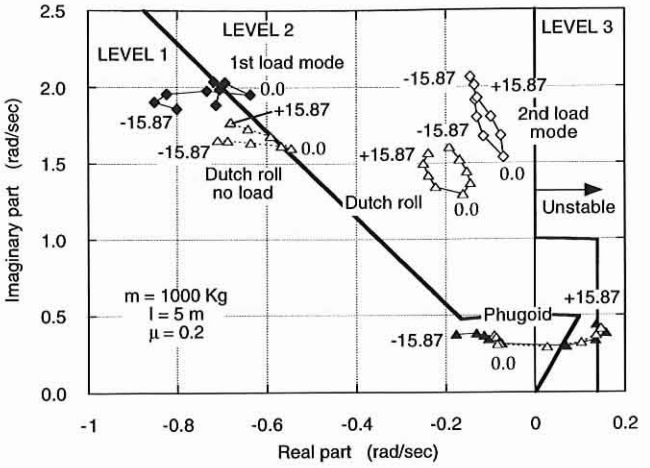


**Fig. 9. Selected aircraft and load poles as a function of turn rate.**

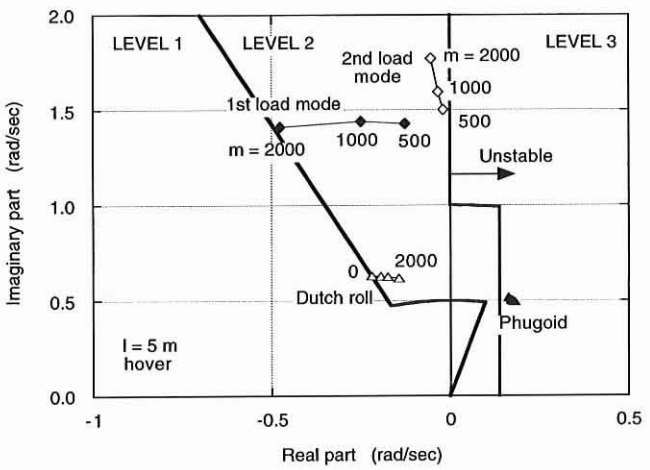


**Fig. 10. Selected aircraft and load poles as a function of load mass.**

Figures 8 through 12 provide stability information in the form of root loci of system poles, namely phugoid, Dutch roll, and two load modes. All the figures show the Level 1, 2, and 3 boundaries for the hover and low-speed mid-term requirements of the ADS-33 specifications (Ref. 1) (the requirements apply only to the helicopter poles, and not to the load poles). In most modes, including those shown in the figure, there is some coupling between the aircraft rigid-body, the rotor flap and lag, and the load degrees of freedom. The load does not degrade the stability of the rotor modes, and therefore no rotor results are presented.

Figures 8 compares the poles with and without the load, as a function of $\mu$, for a 5 meter cable and a 1000 kg load. The phugoid becomes stable in forward flight; the behavior for increasing $\mu$ is almost the same with and without the load. The second load mode is lowly damped. The corresponding pole does not move appreciably with increasing speed. On the other hand, the behavior of the Dutch roll mode is noticeably modified by the presence of the load. The mode that interacts with the Dutch roll is primarily a rotation of the suspended load about the $z_H$ axis. Together with the load azimuth $\phi_L$ the primary component of corresponding load eigenvector is the lateral velocity $v$ of the helicopter. The coupling reduces both the frequency of the Dutch roll mode and its damping, compared with the case without the load. The handling qualities deteriorate accordingly. (However, the limitations of the model due to the simple load aerodynamics should be kept in mind.)

The same interesting coupling between load modes and Dutch roll can be seen in Fig. 9, which shows the poles in turning flight at an advance ratio $\mu = 0.2$, for a cable length of 5 m and a load mass of 1000 kg. The addition of the load reduces both frequency and damping of the Dutch roll. The damping is transferred to the first load mode. The behavior of the phugoid is essentially the same with or without the load; the mode becomes slightly unstable in right-handed turns. Otherwise, the effects of turn rate appear to be modest.

Figure 10 shows the effect of increasing load mass in hover, for a 5 meter cable. The damping of the first load mode increases substantially, while the Dutch roll damping decreases; the handling qualities go from borderline Level 1 to Level 2. The second load mode frequency increases slightly. The phugoid is mostly unchanged. The Dutch roll damping can also decrease by increasing the weight of the helicopter alone, that is, without a slung load. Therefore it may be interesting to distinguish between the case in which the helicopter weight stays constant and the load weight increases (this is the case shown in Fig. 10) and the case in which the helicopter weight is increased without a slung load. For this purpose, the Dutch roll poles were calculated without the load, and with the helicopter mass increased as in Fig. 10, i.e., by 0, 500, 1000, and 2000 kg. In the scale of the figure, the root locus plot (not shown) would be superimposed to that for increasing load mass. However, the pole for a 2000 kg mass increase of the helicopter is essentially coincident with that for a 500 kg mass increase of the load. In other words, increasing the mass of the suspended load causes a decrease in the Dutch roll damping that is about four times that that would be caused by the same increase in the gross weight of the helicopter alone, without the load.

In hover, the poles are only minimally affected by the drag characteristics of the load. For example, for the case of $m = 1000$ kg and $l = 5$ m, the real and imaginary parts of the Dutch roll poles change by about 0.1% and 0.02% respectively as the equivalent flat plate area of the load $S_L$ is changed from 0 to 1.2 m$^2$. The changes are slightly more significant in forward flight. Figure 11 shows the four lowest frequency poles at $\mu = 0.2$ as a function of $S_L$. While the poles of the phugoid, Dutch roll, and first load modes stay largely unchanged, the second load mode becomes more stable as $S_L$ increases. However, the load drag does not change with angle of attack and sideslip: this is an idealized situation, corresponding to a spherical load with no separated flow. The drag of a real load can have a more complex behavior, and increasing the flat plate area will not necessarily increase stability.

Finally, Fig. 12 shows the effect of cable length in hover, for a 1000 kg load. As expected, given the analogy with a pendulum, a longer cable

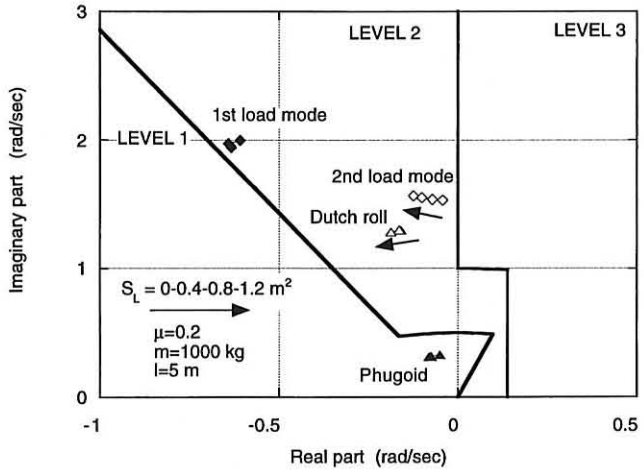


**Fig. 11. Selected aircraft and load poles as a function of equivalent flat plate area $S_L$ of the slung load.**

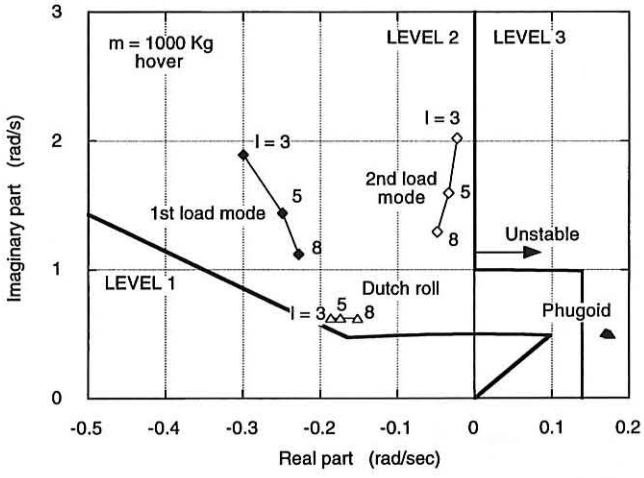


**Fig. 12. Selected aircraft and load poles as a function of cable length.**

lowers the frequency of the load modes. The Dutch roll damping decreases slightly, the phugoid is largely unchanged.

### Frequency response to pilot inputs

This section presents frequency response plots for various load configurations and flight conditions. These plots provide the basic information to assess compliance with the ADS-33 bandwidth specifications (Ref. 1). Because the slung load affects the roll degree of freedom the most, all plots will refer to the roll attitude response to lateral cyclic.

Figure 13 shows the effects of cable length. The primary features introduced by the load are a notch in the gain diagram and a phase shift of approximately 180 degrees. These features occur at a natural frequency of the load, seen as a pendulum. As the length of the cable increases the pendulum frequency decreases, and the features move to lower frequencies. For the parameters used in the study the strongest effects due to the presence of the load are concentrated between 1 and 2 rad/sec. Therefore, they do not affect the frequency $\omega_{180}$ at which the phase curve crosses the 180-degree line. The shape of the gain curve in the frequency range involved in the calculation of the gain bandwidth (Ref. 1) is also essentially unaffected, and therefore the gain bandwidth is not changed by the load. The phase shifts introduced by the load introduce new crossings of

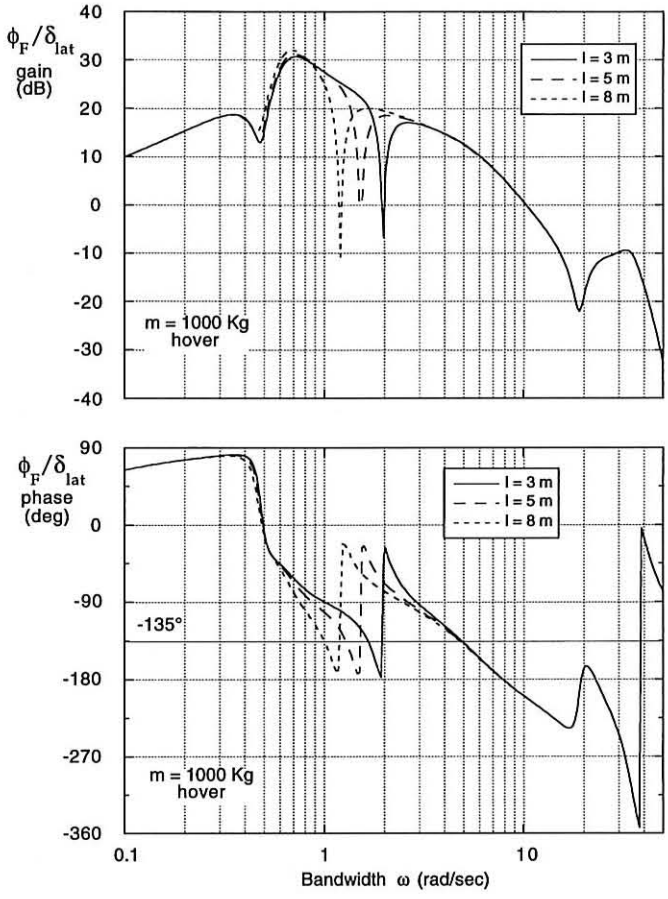


**Fig. 13. Roll attitude frequency response to lateral cyclic as a function of cable length.**

the 135-degree delay line, which determine the phase bandwidth (Ref. 1). These crossings occur between 1 and 2 rad/sec, much lower than that of the "baseline" crossing at about 5 rad/sec. These results alone cannot indicate whether the lower or the higher frequency crossing should be used for the calculation of the phase bandwidth, or, equivalently, whether the load degrades roll handling qualities so substantially. The flight tests of Ref. 9 do indicate some worsening of roll handling qualities and a reduction of bandwidth, although not as dramatic. In the frequency response plots of Ref. 9 the gain notch and the phase shifts at the pendulum frequency are less evident than in the present study. In particular, the flight frequency responses do not show the multiple crossings of the 135-degree line. The probable reason is that the linearized model used in this study corresponds to infinitesimally small inputs, whereas the flight tests were conducted with nonnegligible control inputs (about 10% of the available control range) that engaged the nonlinearities of the systems. Therefore, the frequency responses from flight tests should be considered as a describing function or optimum linear fit to a nonlinear system. Because of these differences between theoretical and experimental frequency responses, any conclusions drawn based on the former should be viewed with some caution.

Some additional insight in the effects of the load can be gained by considering a very simple 2-degree of freedom model of uncoupled roll or pitch dynamics. The model is shown in Fig. A.1, and the relevant equations of motion are provided in the Appendix. Equation (A.5) is a frequency response equation; the corresponding magnitude and phase plots are shown in Fig. 14 as a function of cable length $l$. The behavior in the 1–2 rad/sec frequency band is reproduced qualitatively very well. At

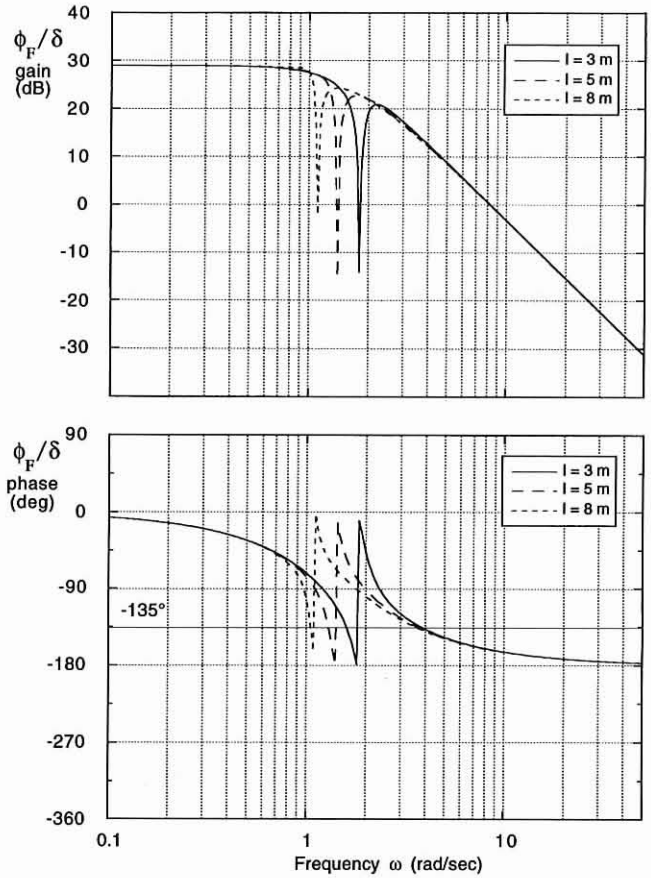


**Fig. 14. Roll attitude frequency response to lateral cyclic as a function of cable length obtained from the simplified helicopter-load model.**

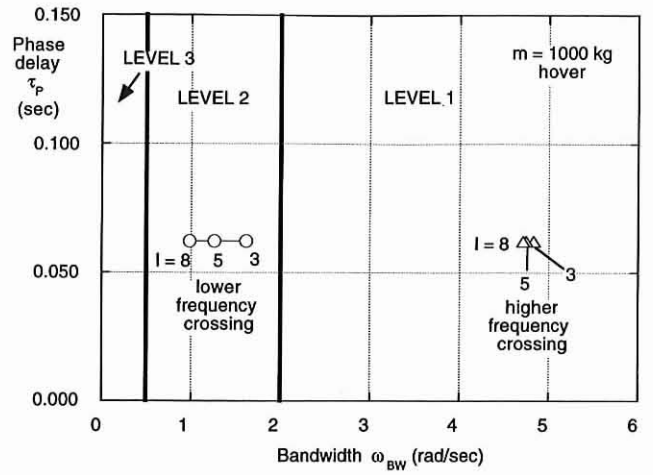


**Fig. 15. Effect of cable length on roll handling qualities.**

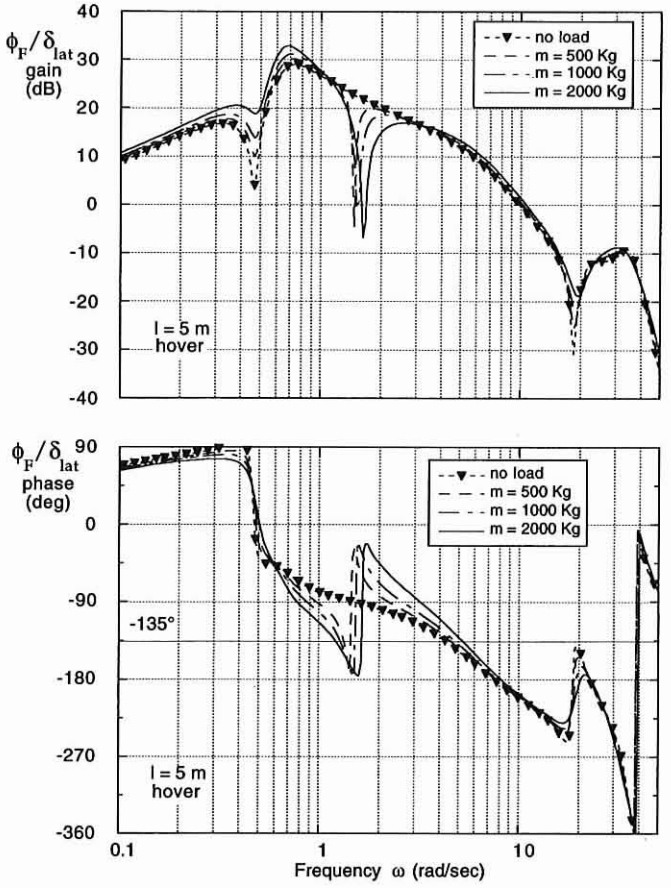


**Fig. 16. Roll attitude frequency response to lateral cyclic as a function of load mass.**

the frequency of the notch the amplitude of the oscillation of the pendulum tends to become extremely large (not shown in Fig. 14) whereas the amplitude of the idealized motion of the helicopter tends to zero. There is no damping in the pendulum motion, and very lowly damped zeros that do not cancel out the load poles, hence the sharp phase shifts. The coupled rotor-fuselage model used in this study also indicates lateral flapping in phase with the lateral oscillations of the load, that is, on the same side of the $x$-$z$ plane.

The effect of cable length on roll handling qualities is summarized in Fig. 15. Because cable length affects neither the value of the $\omega_{180}$ frequency nor the shape of the phase curve beyond $\omega_{180}$, the phase delay is the same regardless of cable length. The figure shows two groups of representative points, corresponding to the lower and the higher frequency crossing of the 135-degree delay line respectively. The latter is probably the more representative because, as previously mentioned, the frequency responses from flight tests do not show the lower frequency crossings (Ref. 9). In this case there is essentially no change in bandwidth, and therefore in handling qualities, which are predicted to be Level 1. If the other set of points was to be considered, then the load would degrade the roll handling qualities to Level 2. In this case, the handling qualities would worsen with increasing cable length.

Figure 16 shows the effects on the roll frequency response of increasing the load mass. The flight condition is hover, and the cable length is $l = 5$ m. The effects are relatively minor, and are mostly related to the increase in the overall weight of the helicopter caused by the load. A slight increase of the $\omega_{180}$ can be seen, as well as a slight gain increase at most frequencies. The phase bandwidth increases by about 1 rad/sec in going from the unloaded to the most highly loaded configuration. There is also a small increase of the frequency of the notch in the gain plots and of the phase jumps.

The effect on roll handling qualities is shown in Fig. 17. As in Fig. 15 two groups of points are shown. The small changes at $\omega_{180}$ and above result in only small changes of phase delay. The overall bandwidth is the phase bandwidth, which increases with increasing load. As in Fig. 15, if the "low crossing-frequency" points are considered, then the slung load

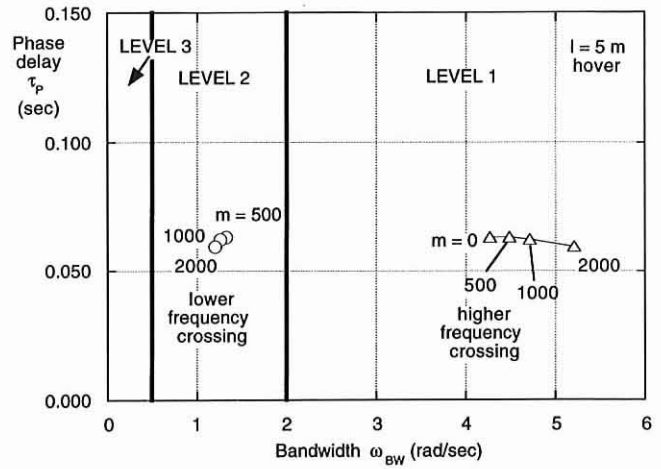


**Fig. 17. Effect of load mass on roll handling qualities.**

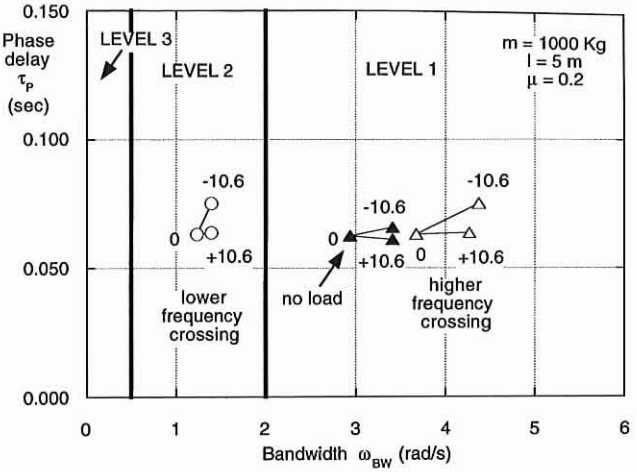


**Fig. 19. Effect of turn rate on roll handling qualities.**

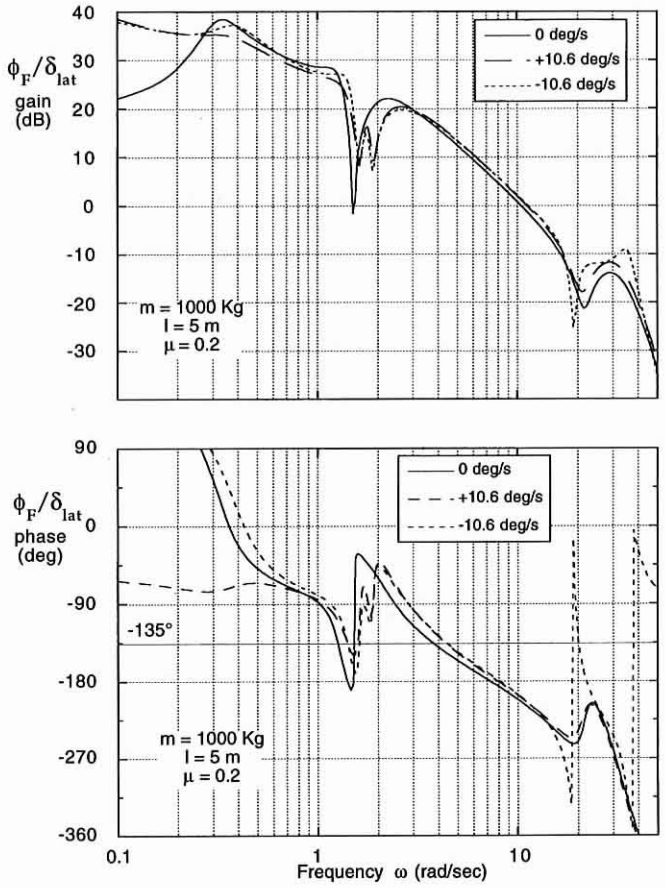


**Fig. 18. Roll attitude frequency response to lateral cyclic as a function of turn rate.**

degrades noticeably the roll handling qualities, which become Level 2. In this case, slightly lower bandwidths and phase delay occur with increasing load mass.

The effect of turning flight can be seen in Fig. 18, which shows the frequency responses at $\mu = 0.2$, for a 1000 kg load and a cable length of 5 m. The turn rates are $\pm 10.6$ deg/sec, corresponding to a load factor $n_T = 1.25$ for the helicopter without the external load, and approximately $n_T = 1.33$ with the load. In both turning flight conditions the notch in the gain plot becomes less pronounced, and it is replaced by two smaller dips. Similarly, the phase jump is less sharp and is composed by two smaller changes. Turn rate increases the coupling between longitudinal and lateral-directional dynamics. As a consequence, pole-zero pairs that would cancel in straight flight no longer do so in turns (Ref. 19). The same occurs for the load modes. The two load modes can be interpreted as an oscillation in the longitudinal plane plus an oscillation in the lateral plane. In the roll transfer function for straight flight, the poles corresponding to the longitudinal load mode are canceled by a pair of zeros and their effect does not appear in the frequency response plots. This pole-zero cancellation is weaker in turning flight, and this results in the changes of the shapes of gain and phase curves that can be observed in Fig. 18. Although interesting from a theoretical point of view, these features are not likely to cause significant changes in handling qualities. Finally, except at the lowest frequencies, no noticeable differences can be seen by replacing the roll angle $\phi_F$ with the integral $\phi_F^*$ of the roll rate $p$ (see Ref. 19 for a discussion of this issue).

The effect on roll handling qualities is shown in Fig. 19. The slung load increases the phase bandwidth, and in this case the overall bandwidth, by about 1 rad/sec both in straight and in turning flight. The "low crossing-frequency" points again indicate that the handling qualities characteristics would degrade to Level 2.

## Summary and Conclusions

The paper presented a study of the flight dynamics and handling qualities of an articulated rotor helicopter carrying a suspended load. The aircraft model included rigid body dynamics, individual flap and lag dynamics of each blade, and inflow dynamics. The external load was modeled as a point mass suspended from a single point, and the only aerodynamic load was a quasi-steady drag force in the direction of the local airflow; no aerodynamic forces acted on the cable. The limitations of the aerodynamic model of the load should be kept in mind in evaluating and generalizing the conclusions of this study.

The main conclusions of the present study are:

1) The load affects trim primarily through the overall increase in the weight of the aircraft, both in straight and in turning flight. The influence of cable length is negligible.

2) Substantial dynamic coupling can occur between the Dutch roll mode and a load mode that consists primarily of the lateral motion of the load. Because of this coupling, the Dutch roll damping can decrease with

a consequent deterioration of handling qualities. The effects of the load on the phugoid are typically very small.

3) Higher order dynamics, such as rotor and inflow dynamics, has a modest effect on the stability of the lowest frequency modes of the aircraft and the load; a quasi-steady rotor model is probably sufficiently accurate for those modes.

4) A suspended load modifies the on-axis roll frequency response by adding a notch to the gain curves and a roughly 180-degree jump in the phase curves. These features occur at the pendulum frequencies of the load, and are associated with a mode with small roll motions of the helicopter, large amplitude lateral load motions, and lateral rotor flapping in phase with the motion of the load.

5) The frequency responses identified from flight test data show smaller gain notches and phase jumps than those calculated from the linearized model of the present study. A possible reason is that the former effectively include some degree of nonlinearity, whereas the latter are strictly linear and correspond to infinitesimally small inputs.

6) The changes of the frequency response introduced by the load occur primarily at frequencies lower than those used to determine bandwidth and phase delay according to the ADS-33 specifications. However, the phase shifts cause additional crossings of the 135-degree delay line that, at least formally, can reduce the phase bandwidth considerably: if these are ignored, the changes in bandwidth and phase delay are small.


### Acknowledgments

The Authors would like to thank the Reviewers for many insightful comments, and for the interpretation of the differences between theoretical and experimental frequency responses.


### Appendix: Idealized Model of Helicopter and Suspended Load

The idealized model is shown in Fig. A.1. The equations of motion of the system are:

$$L_\delta \delta = (I_x + mr^2)\ddot{\phi}_F + m\ddot{\phi}_L rl\cos(\phi_F - \phi_L) - m\dot{\phi}_L(\dot{\phi}_F - \dot{\phi}_L)rl\sin(\phi_F - \phi_L) - m\dot{\phi}_F\dot{\phi}_L rl\sin(\phi_F - \phi_L) + mgr\sin\phi_F - L_p\dot{\phi}_F \quad (A.1)$$

$$0 = ml^2\ddot{\phi}_L + m\ddot{\phi}_F rl\cos(\phi_F - \phi)_L - m\dot{\phi}_F(\dot{\phi}_F - \dot{\phi}_L)rl\sin(\phi_F - \phi_L) - m\dot{\phi}_F\dot{\phi}_L rl\sin(\phi_F - \phi_L) + mgl\sin\phi_L \quad (A.2)$$

When linearized about the equilibrium position $\bar{\theta}_L = \bar{\phi}_F = \bar{\delta} = 0$ with $\cos(\phi_F - \phi_L) \approx 1$ and $\sin(\phi_F - \phi_L) \approx \phi_F - \phi_L$, the system becomes, in perturbation form:

$$L_\delta \Delta\delta = (I_x + mr^2)\Delta\ddot{\phi}_F + mrl\Delta\ddot{\phi}_L + mgr\Delta\phi_F - L_p\Delta\dot{\phi}_F \quad (A.3)$$

$$0 = ml^2\Delta\ddot{\phi}_L + mrl\Delta\ddot{\phi}_F + mgl\Delta\phi_L \quad (A.4)$$

Letting $\Delta\delta(t) = \delta_0 e^{i\omega t}$, $\Delta\phi_F(t) = \phi_{F0}e^{i\omega t}$, and $\Delta\phi_L(t) = \phi_{L0}e^{i\omega t}$, and substituting into Eqs. (A.3) and (A.4) gives, after some manipulations:

$$\left[\left(1 - \frac{k_2}{u^2} + k_2 k_4 \frac{u^2}{1-u^2}\right) + i\left(\frac{L''_p}{\omega}\right)\right]\phi_{F0} = -\frac{L''}{\omega^2}\delta_0 \quad (A.5)$$

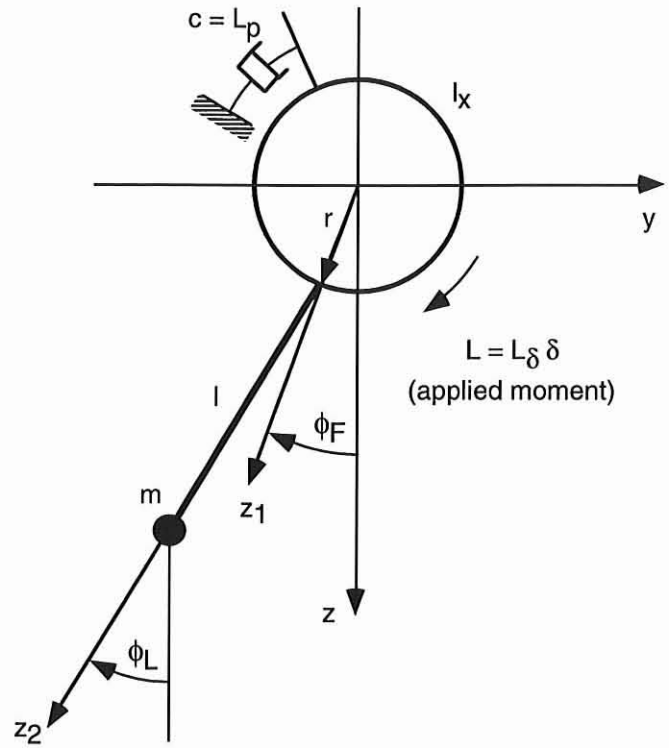


**Fig. A.1. Simplified helicopter-load model.**

where

$$k_1 = \frac{ml^2}{I_x} \qquad k_2 = \frac{k_1\left(\frac{r}{l}\right)}{1 + k_1\left(\frac{r}{l}\right)^2} \qquad L''_p = \frac{\frac{L_p}{I_x}}{1 + k_1\left(\frac{r}{l}\right)^2}$$

$$L''_\delta = \frac{\frac{L_\delta}{I_x}}{1 + k_1\left(\frac{r}{l}\right)^2} \qquad k_4 = \frac{r}{l}$$

and $u = \omega/\omega_P$, where $\omega_P = \sqrt{g/l}$ is the natural frequency of the mass pendulum for $\phi_F(t) = 0$.

### References


[1] Anonymous, "Handling Qualities Requirements for Military Rotorcraft," US Army Aviation and Missile Command, ADS-33D-PRF, May 1996.

[2] Lucassen, L. R., and Sterk, F. J., "Dynamic Stability Analysis of a Hovering Helicopter With A Sling Load," *Journal of the American Helicopter Society*, Vol. 10, (2), April 1965.

[3] Szustak, L. S., and Jenney, D., "Control of Large Crane Helicopters," *Journal of the American Helicopter Society*, Vol. 16, (3), July 1971.

[4] Dukes, T. A., "Maneuvering Heavy Sling Loads Near Hover, Part I: Damping the Pendulous Motion," *Journal of the American Helicopter Society*, Vol. 18, (2), April 1973.

[5] Dukes, T. A., "Maneuvering Heavy Sling Loads Near Hover, Part II: Some Elementary Maneuvers," *Journal of the American Helicopter Society*, Vol. 18, (3), July 1973.

[6] Poli, C., and Cromack, D., "Dynamics of Slung Bodies Using a Single-Point Suspension System," *Journal of Aircraft*, Vol. 10, (2), February 1973.

[7]Cliff, E. M., and Bailey, D. B., "Dynamic Stability of a Translating Vehicle with a Simple Sling Load," *Journal of Aircraft*, Vol. 12, (10), October 1975.

[8]Nagabhushan, B. L., "Low-Speed Stability Characteristics of a Helicopter With a Sling Load," *Vertica*, Vol. 9, 1985.

[9]Cicolani, L. S., McCoy, A. H., Tischler, M. B., Tucker, G. E., Gatenio, P., and Marmar, D., "Flight-Time Identification of a UH-60A Helicopter and Slung Load," *Proceedings of the NATO RTA Symposium on System Identification for Integrated Aircraft Development and Flight Testing*, Madrid, Spain, May 1998.

[10]Sheldon, D. F., "An Appreciation of the Dynamic Problems Associated with the External Transportation of Loads from a Helicopter—State of the Art," *Vertica*, Vol. 1, 1977.

[11]Prabhakar, A., "Stability of a Helicopter Carrying an Underslung Load," *Vertica*, Vol. 2, 1978.

[12]Cicolani, L. S., Kanning, G., and Synnestvedt, R., "Simulation of the Dynamics of Helicopter Slung Load Systems," *Journal of the American Helicopter Society*, Vol. 40, (4), October 1995.

[13]Gabel, R., and Wilson, G. J., "Test Approaches to External Sling Load Instabilities," *Journal of the American Helicopter Society*, Vol. 13, (3), July 1968.

[14]Simpson, A., and Flower, J. W., "Lateral Flutter of Loads Towed Beneath Helicopters and Its Avoidance," *Vertica*, Vol. 5, 1981.

[15]Peters, D. A., and HaQuang, N., "Dynamic Inflow for Practical Applications," *Journal of the American Helicopter Society*, Vol. 33, (4), October 1988.

[16]Chen, R. T. N., and Jeske, J. A., "Kinematic Properties of the Helicopter in Coordinated Turns," NASA Technical Paper 1773, April 1981.

[17]Celi, R., "Hingeless Rotor Dynamics in Coordinated Turns," *Journal of the American Helicopter Society*, Vol. 36, (4), October 1991.

[18]Greenwood, T., *Principles of Dynamics*, Prentice-Hall, 1988, pp. 224–226.

[19]Guglieri, G., and Celi, R., "Some Aspects of Helicopter Flight Dynamics in Steady Turns," *Journal of Guidance, Control, and Dynamics*, Vol. 21, (3), May-June 1998.